CONF-9610256--1

cd rev 1/9/97 Draft.2--Ecole "Dislocations 96" Interfaces and Plasticity (to be submitted)

Role of Interfaces in Deformation and Fracture of Ordered Intermetallics

M. H. Yoo and C. L. Fu

Metals and Ceramics Division, Oak Ridge National Laboratory, Oak Ridge, TN 37831-6115, USA

Abstract : While sub- and grain-boundaries are the primary dislocation sources in $L1_2$ alloys, yield and flow stresses are strongly influenced by the multiplication and exhaustion of mobile dislocations from the secondary sources. The concept of enhanced microplasticity at grain boundaries due to chemical disordering is well supported by theoretical modeling, but no conclusive direct evidence exist for Ni_3Al bicrystals. The strong plastic anisotropy reported in TiAl PST crystals is attributed in part to the localized slip along lamellar interfaces, thus lowering the yield stress for soft orientations. Calculations of work of adhesion suggest that, intrinsically, interfacial cracking is more likely to initiate on γ/γ-type interfaces than on the α_2/γ boundary.

I. Introduction

As compared to fcc metals and alloys, ordered intermetallic compounds of the $L1_2$ structure are generally known to possess high strength at elevated temperatures due to the relatively low atomic diffusivity and dislocation mobility. The anomalous (positive) temperature dependence of yield stress observed in certain ordered intermetallics of relatively high ordering energy, e.g., Ni_3Al [1,2], has been the subject of active research in recent years [3-7]. The role of interfaces in creating the mobile dislocations that are responsible for the yield stress anomaly in $L1_2$ alloys has not been adequately addressed, however, and is one of the objectives of this overview paper.

In addition to this intrinsic thermal strengthening there is also the phenomenon of what has been often assumed to be the "intrinsic" brittleness of grain boundaries (GBs) in ordered intermetallics [8]. This assumption is based on the low value of grain-boundary cohesive energy, which leads to an explanation that the dramatic improvement in room temperature ductility of Ni_3Al by small boron addition and hypostoichiometric deviation [9,10] is due directly to the strengthening of GBs by boron segregation there. An alternative theory based on enhanced slip transfer across GBs has also been proposed, leading to the correlation between the degree of chemical disordering at GBs and localized plasticity at the GBs instead of crack initiation. Experimental and theoretical studies carried out to resolve this controversial issue between the two theories were critically reviewed in the nine papers of a Viewpoint Set [11-19] following the introduction [8]. As a prerequisite to explaining this boron ductilizing effect, it is

important to understand nucleation and growth mechanisms of intergranular fracture in $L1_2$ alloys, without extrinsic effects such as micro- and macroalloying and/or test environment, by examining the cohesive strength of a GB, localized plasticity near the boundary, and the internal stress state. Another objective of this paper is to summarize the crystallographic and physical bases for intergranular fracture, emphasizing the intrinsic interfacial structure and properties.

In the case of Ti-rich two-phase TiAl/Ti_3Al alloys, significant advances have been made recently in understanding the role of interfaces in the deformation and fracture behavior of fully lamellar microstructures, due largely to the controlled experimental investigations using the so-called polysynthetically twinned (PST) crystals [20,21] and the theoretical calculations of bulk and defect properties of the two constituent phases [22-28]. Still another objective of this paper is to interpret available experimental data on the role of interfaces in deformation and fracture of PST TiAl crystals in terms of the calculated results of surface and interfacial energies of various homo- and heterophase interfaces [29].

There arise some difficulties when one makes a direct comparison between theoretical concepts and experimental results. In theory, while any variation in properties due to a change in the binary alloy composition is considered intrinsic to the alloy system, all other changes due to micro- and macroalloying as well as environmental effects are regarded as extrinsic factors. In practice, however, the so-called intrinsic properties are seldom measurable in intermetallic alloys owing to residual trace elements in an alloy system and environmental impurities in a test chamber. High solubility of interstitial oxygen in titanium aluminides and environmental embrittlement effects in Ni_3Al are two outstanding examples. According to a recent review [30], the poor ductility of polycrystalline Ni_3Al tensile tested in ambient air is due mainly to environmental embrittlement, without which these Ni_3Al alloys are now known to be quite ductile. Scarce though the available experimental data may be, we will try to concentrate our discussion on dislocations and interfaces in $L1_2$ alloys and TiAl-based alloys on the basis of their "intrinsic" physical and mechanical properties.

II. Plastic Deformation by Slip

In order to assess the effect of long-range ordering on plastic deformation, a comparative analysis based on the ordered and disordered structures is possible for an alloy in which the order-disorder transition temperature is below its melting point ($T_c < T_m$). Two good examples are the $L1_2$-fcc transition of Cu_3Au at $T_c \approx 0.5\ T_m$ and the $D0_{19}$-hcp transition of Ti_3Al at $T_c \approx 0.7\ T_m$. On the other hand, the ordering energies for the $L1_2$ and $L1_0$ phases, respectively, in Ni_3Al

and TiAl are so high that T_c is above their peritectic and eutectic temperatures [31]. In the case of Ni_3Al a comparison analysis with Ni and Ni-Al alloys of the fcc structure may be attempted.

II.1. Interfaces as Dislocation Sources

Dislocation sources and sinks and multiplication and annihilation mechanisms in metals and alloys were summarized in two excellent review articles [32,33]. In "perfect" crystals with an initial dislocation density of $\rho_o<10^6$ cm^{-2} and no sub-boundaries, the multiplication starts generally from surface sources, and the dislocations traverse paths of the order of the crystal diameter. The critical resolved shear stress (CRSS) is smaller than the Frank-Read (F-R) stress calculated for dislocation segments between grown-in dislocations, since surface sources can be activated more easily. In imperfect crystals with $\rho_o>10^6$ cm^{-2}, on the other hand, dislocation multiplication starts first at sub-boundaries of minimum misorientation. The CRSS of these crystals is of the order of the F-R stress calculated for the sub-boundary sources, and the glide paths are of the order of a few times the subgrain diameters. In polycrystals each grain behaves similarly to an imperfect crystal.

An overview of the current understanding of dislocation sources and multiplication mechanisms for ordered intermetallic alloys of the $L1_2$, B2, and $D0_{19}$ structures was made recently [34]. The highlights of this overview relating to $L1_2$ alloys are summarized below.

II.1.1 $L1_2$ Alloys

Using *in situ* straining electron and optical microscopic observations, Takeuchi et al. [35] observed in Ni_3Ga single crystals multiplication process of superdislocations (dislocations, hereon) starting from sub-boundaries, as shown schematically in Fig. 1. Dislocation motion of the (111)[101] slip system at low temperatures (≤500 K) was so quick and jerky that a direct recording of the slip process was not possible with the available resolution of 0.03 s. Once dislocations were multiplied on the {111} plane, they seldom moved again on the same plane when they were oriented along the <101> screw direction. Essentially, the same features were observed also in Ni_3Al single crystals by Nemoto et al. [36]. More recent work of *in situ* straining weak-beam transmission electron microscopy (TEM) investigation on Ni_3Al [4] revealed the so-called "locking-unlocking" behavior of screw dislocations when they moved at 300 K.

Curved configuration of {111}<101> dislocations in $L1_2$ alloys has been investigated in details by post-mortem TEM [3,7]. The schematic drawing of Fig. 2(a) illustrates that either the

cross-slip pinning (CSP) of the outer superpartials [5] (the top half) or the immobilization by a Kear-Wilsdorf (K-W) lock (the bottom half) causes the elongated shape of a glide loop containing a distribution of macro-kinks or the so-called super-kinks. A high propensity for the formation of long cross-slipped segments terminated by super-kinks was predicted by a dynamical simulation of the motion of {111}<101> dislocations [6]. Between the two adjacent long screw segments, secondary dislocation sources may be activated from super-kinks, as illustrated schematically in Fig. 2(b), provided that the local stress is sufficiently high for the F-R stress.

On the basis of the *in-situ* high-voltage electron microscopy (HVEM) observations [35,36], it may be concluded that the macroscopic yield stress (0.2% proof stress) in Ni_3Ga or Ni_3Al is determined by the activation of slip band sources (i.e., sub-boundaries as the primary dislocation sources) rather than the mobility of multiplied dislocations. On the other hand, the major conclusion from the recent post-mortem TEM [3,7] and dislocation dynamical analyses [6] is that the principal role of cross-slip of screw dislocations is not in the reduction of dislocation velocity, but rather in the exhaustion of the density of mobile dislocations by raising the back stress exerted on the secondary dislocation sources. While these conclusions both emphasize the importance of multiplication of slip dislocations rather than their mobility, there are some important differences between the two insofar as the macroscopic yield and flow behavior is concerned.

First, there are geometrical difficulties associated with expansion of the elongated primary glide loops. When the loops expand primarily along one direction, in the direction of Burgers vector by the motion of mobile edge dislocations, as shown in Figs. 1 and 2(a), the critical stage for first revolution of F-R source anchored around the nodes located at a sub-boundary with the spacing of l_0 would be extremely difficult to reach. On the contrary, the critical stage of a secondary source, Fig. 2(b), can be overcome by the aid of dipole formation on a super-kink when the long screw segments cross slip into the cube plane [3,7]. Therefore, while the primary sources of mobile dislocations at sub-boundaries may make a significant contribution to the yield stress, presumably in the early micro-yielding regime, it is the secondary sources at the super-kinks that may be responsible for the yield and flow stresses, and hence the yield stress anomaly in certain $L1_2$ alloys.

II.1.2 TiAl Alloys

For the ordinary slip with the <110]/2 vector in γ-phase TiAl alloys, a single-ended F-R source developed from a jogged screw dislocation has been observed at room temperature, and different

variants of the classical Bardeen-Herring dislocation climb sources at elevated temperatures [37]. In two-phase PST crystals, on the other hand, all the variants of γ/γ and the α_2/γ semicoherent interfaces are the primary multiplication sites for dislocations [37]. The internal stresses that will effect these interfaces as dislocation sources are induced by the misfit strain due to the lattice mismatch and the thermoelastic mismatch.

After relaxation by the creation of van der Merwe misfit dislocations, diffusion across the interfaces, and cracking along the interfaces, these stresses are estimated to be of the order of 100 MPa according to the measurements of lattice parameters by Convergent Beam Electron Diffraction (CBED) technique [38]. The residual coherency stresses were determined to be in the range of 20-220 MPa by analyzing the curvature of dislocation loops which were emitted from the network of interfacial dislocations [39]. *In situ* heating cycle of 300-994-300 K was found to generate dislocations at lamellar interfaces, which gives an estimate of 70 MPa as the incremental thermoelastic stress [40]. In contrast, the additional induced stress in Ti_3Al of a PST crystal due to the elastic incompatibility between TiAl and Ti_3Al was estimated to be relatively small, viz., -9 % of an applied stress normal to the interface and +4 % in the parallel direction [27].

II.2. Interaction of Slip with Interfaces

Figure 3 shows schematically slip-interface interactions which may lead to slip transfer and/or initiation (top half) and cleavage or interfacial crack nucleation (bottom half). The latter will be referred to in Sec. III. While the dislocations initiating from sub-boundaries or semicoherent lamellar interfaces discussed above are the special cases of the upper-right of Fig. 3, GBs in general may be also included in the present discussion.

A lattice dislocation can be absorbed into a GB as shown in the upper left of Fig. 3. According to the coincident-site-lattice (CSL) theory of GBs, the Burgers vector of each lattice dislocation may be decomposed into an integer multiple of displacement shift complete (DSC) vectors. Also, for the case of slip transfer or transmission, an extrinsic GB dislocation (EGBD) [41] resulting from the process must have a total Burgers vector strength equal to an integer multiple of DSC vectors in order for the conservation of Burgers vectors to be maintained. Other indirect transmission or reflection, such as absorption of lattice dislocations at a GB site causing emission of dislocations at another site, across the interface or within the same grain, is merely a combination of the two basic processes, absorption (or initiation) and transmission.

II.2.1 Dislocation Reactions in $L1_2$ Alloys

Numbers of allowable dislocation reactions at GBs between the $L1_2$ and fcc crystal structures were carried out earlier [42] by considering a total of 30 independent Burgers vectors of superpartials, <101>/2, Shockley partials, <112>/6, and super-Shockley partials, <112>/3. The results shown in Table 1 indicate that many of the possible dislocation reactions at GBs become energetically unfavorable if chemical coordination must be maintained in the structure of the GB. For those boundaries with $\Sigma=3N$ (Σ is the volume ratio of the coincident unit to the crystal unit, and N is an integer) the number of permissible dislocation reactions is reduced by a factor of four as the crystal structure is changed from fully disordered (fcc) to ordered (pc). When $\Sigma\neq3N$, on the other hand, the number of permissible transmission reactions is reduced by a factor of three, but no absorption (or initiation) reaction is allowed when the GB region is fully ordered. This result suggests that localized compositional disordering (hypostoichiometric, or Ni-rich Ni_3Al) at the vicinity of GBs may facilitate dislocation emissions from high-angle GBs, thus enhancing generalized plasticity of a polycrystalline alloy.

There are several possible mechanisms by which GB disordering may contribute to improved interfacial ductility: (a) for a given Σ value the DSC lattice of the fcc structure is finer than that of the $L1_2$ structure, (b) the smaller the Burgers vector of product dislocations, the lower the elastic energy of a dislocation reaction, (c) the relatively lower elastic constants at the GB region, (d) the smaller back-stress on following dislocations in a pile-up, and (e) the easier motion of EGBDs by a mixed glide-climb motion, which is the most important means of relieving the back stress.

While experimental evidence for localized disordering at a coherent twin boundary in Cu_3Au exist [43], no conclusive evidence for compositional disordering is available for GBs of Ni_3Al alloys [13-19]. In general, TEM observations of dislocation pile-ups and cracks in Ni_3Al polycrystals were made without performing GB character analyses. A few exceptions are cited below. A high resolution TEM study on a $\Sigma=5$ (130) "tilt" boundary showed no detectable region of compositional disorder [19]. Several different large-angle GBs, with misorientation close to $\Sigma=39b$, $\Sigma=15$ and $\Sigma=3$, in a boron-doped alloy did not show any degree of disordering [44]. Small-angle twist, mixed, and tilt boundaries ($\theta \leq 7°$), and large-angle twist boundaries (near $\Sigma=5$) were ordered up to the vicinity of the interface, but a disordered region of $\approx$1.5 nm thickness was present at a large-angle GB doped with boron [18].

In general, the concept of localized disordering at GBs has been supported by theoretical modeling analyses. For example, the cohesive energies of GBs (Σ=13 twist and tilt, and Σ=15 tilt) determined by the embedded atom method (EAM)-Monte Carlo (MC) simulation were found to be comparable for Ni and Ni_3Al [11]. This result points out the importance of localized plasticity in explaining the degree of GB brittleness. Another MC simulation study showed that only partial disordering of the planes immediately adjacent to the Σ=5 (130) boundary occurred in Ni-rich Ni_3Al alloys both with and without boron [19]. An atomic simulation using the Finnis-Sinclair type potential showed that the "intrinsic" brittleness of a Σ=5 (130) GB is related to the formation of atomic size cavities, as a part of the structural unit, in an $L1_2$ alloy of high ordering energy such as stoichiometric Ni_3Al [11].

II.2.2 Plastic Anisotropy in TiAl Crystals

Yield strength and tensile elongation of PST TiAl crystals are strongly orientation dependent [45]. While in the hard orientation of $\Phi = 90°$ (Φ is the angle between the lamellar plane and the uniaxial loading direction) the yield stress is in excess of 500 MPa and tensile elongation is essentially zero , the yield stress of about 100 MPa associated with 20 % ductility is obtained at a soft orientation ($\Phi = 30°$). This strong plastic anisotropy is attributed, in part, to the marked difference in yield strength between Ti_3Al and TiAl [44]. Since the yield stresses at the soft orientations ($\Phi = 30°$-$51°$) are lower than those of single-phase γ-TiAl alloys at some orientations [46,47], the role of both α_2/γ and γ/γ interfaces in slip and twinning behavior in PST crystals needs to be examined more in detail.

Table 2 summarizes our recent first-principles calculations of interfacial energies and fault energies, including atomic relaxation [29,48]. The pseudo-twin boundary energy is highest, Γ_P = 270 mJ/m^2, and the true-twin boundary energy is lowest, Γ_T = 60 mJ/m^2. Planar fault energies at pseudo-twin and 120°-rotational interfaces are markedly different from those in the bulk γ-phase. That is, the anti-phase boundary (APB) and complex stacking fault (CSF) energies, E_{APB} and E_{CSF}, decrease by about half and the superlattice intrinsic stacking fault (SISF) energy, E_{SISF}, increases approximately threefold.

A comparison analysis of the shear fault energies in the bulk (α_2-phase) and at the two-phase interface was made earlier [28], and the results are shown in Table 3. The shear fault energies at the α_2/γ interface are found to be lower than those on the crystallographic habit planes, (0001) and (111), in the bulk α_2-phase and γ-phase, respectively.

An ordinary dislocation of Burgers vector, $[1\bar{1}0]/2$, is dissociated into a pair of Shockley partials on either the (111) or $(\bar{1}\bar{1}1)$slip plane by ,

$$[1\bar{1}0]/2 \rightarrow [2\bar{1}\bar{1}]/6 + \text{CSF} + [1\bar{2}1]/6, \quad (1)$$

where $E_{CSF} = 530\ mJ/m^2$ in the γ-bulk gives the equilibrium width of d = 0.23 nm at the screw orientation. This is schematically illustrated in the γ_I matrix in the middle of Fig. 4. Due to the lower values of E_{CSF} at the γ/γ-type interfaces (the last column of Table 2) and at the α_2/γ interface (the bottom row of Table 3), relatively wider dissociations at the interfaces are expected, the widest being at the α_2/γ interface with d = 0.55 nm (if the same elastic interaction between the partials as in γ-bulk is assumed). According to the classical Peierls concept (the wider the dissociation configuration of a dislocation, the more mobile the dislocation is), the mobility of $[1\bar{1}0]/2$ screw dislocation is expected to be slightly reduced along a true-twin boundary, but significantly enhanced along all other types of interface when its glide plane is confined along the interface (i.e., "soft" mode dislocations). On the other hand, for shear deformation proceeding on the $(\bar{1}\bar{1}1)$ plane intersecting the lamellar interfaces, the interfaces can act as an effective barrier, thus impeding propagation of slip across the interfaces (i.e., "hard" mode dislocations).

Because of more complex dissociation configuration, involving all three types of the planar faults, the role of interfaces in the relative mobility of superdislocations of <101] Burgers vector is more complicated than of ordinary dislocations. As far as ordinary dislocations are involved, the enhanced mobility along these lamellar interfaces supports the notion of "channeled dislocation motion" [49] or "supersoft deformation mode" [50] in lamellar TiAl. A recent experimental investigation by Kad and Asaro [51] provides a direct evidence of γ/γ interface sliding in PST-TiAl deformed in compression at room temperature.

III. Twinning and Microcrack Nucleation

The top-half of Fig. 3 represents the onset of plastic deformation of one grain (right) under the influence of slip-interface interaction from the adjacent grain (left), which may give rise to a Hall-Petch type relationship for the yield stress. Alternatively, a situation may favor the nucleation of microcrack of either cleavage or interfacial type, as shown in the bottom-half of Fig. 3, which may be controlled by Stroh's mechanism.

In general, nucleation of microcracks at a GB depends on the cohesive energy, G_c, localized plasticity near the GB, and the internal stress state. The cohesive energy related to a cleavage crack is $G_c = 2\gamma_s$, where γ_s is the surface energy. Whereas, the cohesive energy of a specific GB, $G_b = 2\gamma_s - \Gamma_b$ (Γ_b is the GB energy), depends on the GB character and structure and

its chemical state of long-range order (intrinsic effect) and solute segregation (extrinsic effect). The energy dissipation by localized plastic deformation is directly controlled by the stability and mobility of lattice dislocations and EGBDs. In addition, twin nucleation may intervene as a competitive process against the microcrack nucleation, depending on appropriate material properties. For instance, while deformation twinning of the {111}<112>/6 system is inherently difficult in the $L1_2$ structure because of the necessary interchange shuffling on every other twin plane [52], it becomes an important deformation mode in the $L1_0$ structure [53], particularly in γ-TiAl with the low true-twin boundary energy of $\Gamma_T = 60$ mJ/m^2 (Table 2).

III.1 Grain Boundaries

On the basis of the theory of dislocation pile-ups [54], the critical shear stress necessary for microcrack nucleation was expressed earlier [55], for a special two-dimensional case, as

$$\tau_c = \pi\,(A/2l)^{1/2}\,[G_c(\phi)/H(\phi)]^{1/2}, \qquad (2)$$

where l is the length of a dislocation pile-up, $A = Kb/2\pi$, K is the energy factor and b is the magnitude of Burgers vector of a dislocation, and H is the orientation-dependent stress-concentration factor in terms of the angle, ϕ, defined as in Fig. 3. The higher the ratio of two orientation-dependent factors, H/G_c, the easier the crack nucleation would be. The orientation dependence of H with respect to ϕ is shown in Fig. 5. When dislocations in the primary slip system, $(1\bar{1}1)[10\bar{1}]$ are parallel to the [110] tilt axis, they have the mixed character ($\beta = 60°$). The ratio of the energy factor for edge component to that of screw is $K_e/K_s = 1.8$. Nucleation of the most general mixed mode (I-II-III) crack is much more likely than of the pure mode-I crack, particularly at low angles ($\phi < 70.5°$), as far as the stress concentration is concerned.

Surface energies of the {111}, {100}, and {110} potential cleavage planes were calculated by atomistic simulations using the EAM for several fcc metals [56,57] and Ni_3Al [58] (Table 4). Since the {100} and {110} planes in Ni_3Al are composed of alternating mixed Ni-Al planes and pure Ni planes, the cohesive energies for these two cleavage planes are the sums of the two values of surface energy listed in Table 4. The GB cohesive energy listed in Table 4, $\langle G_b \rangle$, is the average value of G_b's for eleven [001] symmetric tilt boundaries [56]. The ratios of the calculated H's and these cohesive energies, viz., $2H/G_c$ and $2H/G_b$, are listed in Table 5 for nine different [110] symmetric tilt boundaries.

The most important conclusion of this calculation was the prediction of cleavage crack initiation in Ni_3Al rather than intergranular cracking [55]. In all cases, but for Σ=17b, (111) cleavage crack nucleation was predicted. When a symmetric double pile-up happens to occur, in

which case the magnitude of H can be doubled, intergranular fracture is possible in most cases considered in Table 5. There are still exceptions, i.e., Σ=19a and Σ=33a. Experimental information on how intergranular fracture depends on the GB character is scarce and limited to only a few materials [59], e.g., Ni_3Al [60], and controlled experiments using bicrystals samples of Ni_3Al have not been performed.

III.2 Heterophase Interfaces

Using the ideal cleavage energies, G_c, calculated earlier [27] and the interfacial energies, Γ_i, obtained recently [29], one can evaluate interfacial fracture energy, the work of adhesion, by

$$G_i = G_c - \Gamma_i - E_m, \qquad (3)$$

where E_m is the misfit energy estimated using the Frank and van der Merwe method [61]. The calculated results are summarized in Table 6. Because of the approximations involved in determining the interfacial and misfit energies, the final interfacial fracture energies are only estimates. Nevertheless, these results enable us to set a relative measure of interfacial fracture mode.

According to the calculated interfacial fracture energies (Table 6), cleavage cracking is least likely to occur on true-twin boundaries and most likely on α_2/γ boundaries. While this is consistent with the recent experimental findings of three-point bending tests of Chevron-notched PST crystals of TiAl [62], a more recent work shows (0001) cleavage within the α_2 phase [63]. In the fracture tests using microcompact tension specimens of TiAl PST crystals [21], it was found that a microcrack was initiated on the α_2 plate and easily developed into a main crack on the (0001) plane, finally leading to failure because of the hydrogen embrittlement of the α_2 phase. Though the intrinsic cleavage energy of the (0001) plane in the α_2 phase is, G_c = 4.8 J/m^2 [27], higher than those of any other interfaces listed in Table 6, it could be reduced appreciably, below the value of 3.8 J/m^2, due probably to the relatively high solubility of interstitials (hydrogen, in this case) in the α_2 phase.

Deformation twinning by {111}<112]/6 and ordinary slip by {111}<110]/2 are the two primary modes of plastic deformation in two-phase TiAl/Ti_3Al alloys at room temperature. Just as for the ordinary slip dislocations, both γ/γ and α_2/γ interfaces are predominantly the sites for twin nucleation. Across γ/γ domain boundaries of pseudo-twin or 120°-rotational type, slip-twin (or twin-slip) transfer often takes place during the soft-mode deformation [45]. The essence of interfacial sites for nucleation of deformation twins is further reinforced by the

recent experimental results on single-phase γ-Ti-56%Al single crystals showing that twinning is much more difficult in the absence of lamellar interfaces [46,47].

Once a cleavage crack is nucleated in TiAl, a coplanar process zone consisting of ordinary slip dislocations and true-twinning partial dislocations may form at the crack tip. This is because of the fact that a {111} plane is not only of the lowest cleavage energy [27], but also the slip and twinning plane. Therefore, a (111) cleavage crack may propagate across a series of γ/γ interfaces under the influence of mode-II and mode-III components of external loading applied to the coplanar $(111)[1\bar{1}2]$twinning (edge) and $(111)[1\bar{1}0]$ ordinary slip (screw), leading to translamellar fracture. This effect of mode mixity was illustrated in terms of crack-tip stress fields [27] and directly observed in a TEM investigation [64].

IV. Discussion

In polycrystalline single-phase intermetallic alloys, grain boundaries are the most important interfaces because they offer the sites not only for dislocation emission and absorption, but also for microcrack initiation. Yield strengths of polycrystalline $L1_2$ alloys generally exhibit the Hall-Petch relation, i.e., the strength dependence on the reciprocal square root of grain size. In $L1_2$ alloys that exhibit yield stress anomaly such as Ni_3Al, Ni_3Si, and Ni_3Ga, etc., the peak stress in a yield stress vs. temperature plot from a polycrystalline sample may be obscured due to this additional GB hardening effect at low temperatures.

As far as the yield stress of PST TiAl crystals is concerned, the apparent Hall-Petch relation was first observed with respect to the γ/γ interfacial spacing in the samples at the hard orientation of $\Phi = 90°$ [65], and this was discussed as a contributing factor to the orientation dependent yield and fracture observed in the PST crystals [49, 66]. According to the model based on the Hall-Petch theory applied to both cases of the soft and hard modes [67], the most important, but the least understood, material parameter was recognized to be the so-called τ^*, the shear stress needed to push a dislocation across the interfaces. More recently, an exceptionally high yield strength, together with relatively high fracture toughness, has been obtained in fully lamellar Ti-47Al-2Cr-2Nb (in atom %) alloys with fine grain size and lamellar spacing [68]. The yield strength at room and elevated temperatures was shown to be sensitive to interlamellar spacing, increasing in strength with decreasing colony size (PST crystalline sub-grain size). In this case of fully lamellar polycrystalline microstructure, where three different length scales (lamellar spacing, colony size, and grain size) are involved, the Hall-Petch relation will not necessarily apply and a more extended series of dislocation pile-up modeling is needed [69].

So far, the interaction of slip with interfaces has been discussed in terms of a dislocation pile-up model under a static equilibrium condition. This model cannot be applied to treat dynamic or quasi-static aspect of a stress concentration, which may strongly influence the effect of temperature and strain rate on yield stress and fracture strain of polycrystalline or multilayered materials. A preliminary analysis indicated that kinetics of dislocation reactions at an interface resulting from the leading dislocation of a pile-up is far more important than any energetic factors involved [70]. In other words, how effectively the reaction products move away from the site of intersection (Fig. 3) seems to be crucial to whether or not the following dislocations can be incorporated into the interface.

V. Summary

In this review paper, the role of interfaces in deformation and fracture behavior in ordered intermetallic alloys was discussed by taking $L1_2$ alloys and titanium aluminides as example cases. The major findings are summarized as follow:

1. In $L1_2$ single crystals, sub-boundaries are the primary sources for dislocations, and the macroscopic flow stress is controlled by the multiplication and exhaustion mechanisms for mobile dislocations.

2. While the role of chemical ordering in localized plasticity at grain boundaries is well established theoretically for the $L1_2$ structure and confirmed experimentally for Cu_3Au, no conclusive direct evidence exist for Ni_3Al bicrystals and polycrystals.

3. In Ti-rich two-phase TiAl PST crystals, semicoherent interfaces are the main dislocation sources, and the localized deformation by ordinary slip, preferentially along the two γ/γ-type and the α_2/γ lamellar boundaries, lowers the yield stresses at soft orientations, contributing to the plastic anisotropy.

4. The effect of mode mixity in TiAl (i.e., mode-III and mode-II loading components on a mode-I crack) is to induce coplanar slip and twinning, leading to translamellar fracture on $\{111\}$ planes across γ_1/γ_2 interfaces.

5. According to the calculated work of adhesion, in two-phase TiAl alloys, interfacial cracking is intrinsically more likely to be initiated on γ/γ-type interfaces than on α_2/γ boundaries.

Acknowledgments

The authors thank E. P. George and J. A. Horton for helpful discussions and Connie Dowker for manuscript preparation. This research was sponsored by the Division of Materials Sciences, U.S. Department of Energy under contract number DE-AC05-96OR22464 with Lockheed Martin Energy Research Corp.

References

[1] Westbrook J. H., *Trans AIME*, **209** (1957) 898.
[2] Flinn P. A., *Trans. AIME*, **218** (1960) 145.
[3] Sun Y. Q. and Hazzledine P. M., *Dislocations in Solids*, F.R.N. Nabarro and M. S. Duesbery Eds., **10,** North Holland Publ. Co. (1996) in press.
[4] Caillard D. and Couret A, *ibid.*, in press.
[5] Vitek V., Pope D. P. and Bassani J. L., *ibid.*, in press.
[6] Chrzan D. C. and Mills M. J., *ibid.*, in press.
[7] Veyssière P. and Saada G., *ibid.*, in press.
[8] Liu C. T., *Scr. Metall. Mater.* **25** (1991) 1231.
[9] Aoki K. and Izumi O., *J. Japan Inst. Met.* **43** (1979) 1190.
[10] Liu C. T., White C. L. and Horton J. A., *Acta Metall.* **33** (1985) 213.
[11] Vitek V. and Chen S. P., *Scr. Metall. Mater.* **25** (1991) 1237.
[12] Takasugi T. and Izumi O, *ibid.*, 1243.
[13] King A. H., Frost H. J. and Yoo M. H., *ibid.*, 1249.
[14] Schulson E. M. and Baker I., *ibid.*, 1253.
[15] George E. P., White C. L. and Horton J. A., *ibid.*, 1259.
[16] Lee T. C., Subramanian R., Robertson I. M. and Birnbaum, H. K., *ibid.*, 1265.
[17] Brenner S. S. and Hua M.-J., *ibid.*, 1271.
[18] Kung H., Rasmussen D. R. and Sass S. L., *ibid.*, 1277.
[19] Mills M. J., Goods S. H., Foiles S. M. and Whetstone J. R., *ibid.*, 1283.
[20] Fujiwara T., Nakamura A., Hosomi M, Nishitani S. R., Shirai Y. and Yamaguchi M., *Phil. Mag. A*, **61** (1990) 591.
[21] Nakano T., Kawanaka T., Yasuda H. Y. and Umakoshi Y., *Mater. Sci. Eng.* **A 194** (1995) 43.
[22] Yoo M. H. and Fu C. L., *Structural Intermetallics*, R. Darolia, J. J. Lewandowski, C. T. Liu, P. L. Martin, D. B. Miracle and M. V. Nathal Eds., TMS Publ., Warrendale, PA (1993) 283.
[23] Rao S. I., Woodward C., Simmons J. P. and Dimiduk D. M., *High-Temperature Ordered Intermetallic Alloys VI*, J. A. Horton, I. Baker, S. Hanada, R. D. Noebe and D. S. Schwartz Eds., MRS Symp. Proc. **364**, MRS Pittsburgh, PA (1995) 129.
[24] Simmons J. P., Mills M. J. and Rao S. I., *ibid.*, 137.
[25] Girshick A. and Vitek V., *ibid.*, 145.
[26] Panova J. and Farkas D., *ibid.*, 151.
[27] Yoo M. H., Zou J. and Fu C. L., *Mater. Sci. Eng.* **A192/193** (1995) 14.
[28] Fu C. L., Zou J. and Yoo M. H., *Scr. Metall. Mater.* **33** (1995) 885.
[29] Yoo M. H. and Fu C. L., *Processing and Design Issues in High Temperature Materials*, N. S. Stoloff and R. H. Jones Eds., TMS Publ., Warrendale, PA (1996), in press.
[30] George E. P. and Liu C. T., *High-Temperature Ordered Intermetallic Alloys VI*, J. A. Horton, I. Baker, S. Hanada, R. D. Noebe and D. S. Schwartz Eds., MRS Symp. Proc. **364**, MRS Pittsburgh, PA (1995) 1131.
[31] *Binary Alloy Phase Diagrams*, T. B. Massalski, ASM, Metals Park, OH (1986).
[32] Li J.C.M., *Dislocation Modeling of Physical Systems*, M. F. Ashby, R. Bullough, C. S. Hartley and J. P. Hirth Eds., Pergamon Press, Oxford (1980) 498.
[33] Neuhäuser H., *Dislocation in Solids*, F.R.N. Nabarro Ed., **6**, North Holland Publ. Co. (1983) 319.

[34] Yoo M. H., Appel F., Wagner R. and Mecking H., *Deformation and Fracture of Ordered Intermetallic Materials*, W. O. Soboyejo, H. L. Fraser and T. S. Srivatsan Eds.,TMS Symp. Proc., Warrendale, PA., in press.
[35] Takeuchi S., Suzuki K. and Ichihara M.,*Trans. Japan Inst. Metals* **20** (1979) 263.
[36] Nemoto M., Echigoya J. and Suto A., *Nippon Kinzoku Gakkaiji* **8** (1980) 925.
[37] Yoo M. H., Appel F., Wagner R. and Mecking H., to be published.
[38] Hazzledine P. M., Kad B. K., Fraser H. L. and Dimiduk D. M., *Intermetallic Matrix Composites II*, D. B. Miracle, D. L. Anton and J. A. Graves Eds., MRS Symp. Proc. **273**, MRS Pittsburgh, PA (1992) 81.
[39] Appel F., Christoph U. and Wagner, R., *Interface Control of Electrical, Chemical, and Mechanical Properties*, S. P. Muraka, K. Rose, T. Ohmi and T. Seidel Eds., MRS Symp. Proc. **318**, MRS Pittsburgh, PA (1994) 691.
[40] Appel F. and Wagner R., *Gamma Titanium Aluminides*, Y.-W. Kim, R. Wagner, and M. Yamaguchi Eds., TMS Symp. Proc., Warrendale, PA (1995) 231.
[41] Priester L. in these Proceedings.
[42] King A. H. and Yoo M. H., *Scr. Metall.* **21** (1987) 1115.
[43] Tichelaar F. D. and Schapink F. W., *Phil. Mag. A* **63** (1991) 207.
[44] Forwood C. T. and Gibson M. A., *Phil. Mag. A* **66** (1992) 1121.
[45] Yamaguchi M. and Inui H., *Structural Intermetallics*, R. Darolia, J. J. Lewandowski, C. T. Liu, P. L. Martin, D. B. Miracle and M. V. Nathal Eds., TMS Publ., Warrendale, PA (1993) 127.
[46] Whang S. H., Wang Z. M. and Li Z. X., *Gamma Titanium Aluminides*, Y.-W. Kim, R. Wagner and M. Yamaguchi Eds., TMS Symp. Proc., Warrendale, PA (1995) 245.
[47] Yamaguchi M, Inui H., Kishida K., Matsumuro M. and Shirai Y., *High-Temperature Ordered Intermetallic Alloys VI*, J. A. Horton, I. Baker, S. Hanada, R. D. Noebe and D. S. Schwartz Eds., MRS Symp. Proc. **364**, MRS Pittsburgh, PA (1995) 3.
[48] Fu C. L. and Yoo M. H., *Scr. Mater.* (submitted).
[49] Kad B. K., Hazzledine P. M. and Fraser H. L., *High-Temperature Ordered Intermetallic Alloys V*, I. Baker, R. Darolia, J. D. Whittenberger and M. H. Yoo Eds., MRS Symp. Proc. **288**, MRS Pittsburgh, PA (1993) 495.
[50] Rao S. I., Woodward C. and Hazzledine P. M., *Defect-Interface Interactions*, E. P. Kvam, A. H. King, M. J. Mills, T. D. Sands and V. Vitek Eds., MRS Symp. Proc. **319**, MRS Pittsburgh, PA (1994) 285.
[51] Kad B. K. and Asaro R. J., unpublished results.
[52] Yoo M. H., *J. Mater. Res.* **4** (1989) 50.
[53] *Twinning in Advanced Materials*, M. H. Yoo and M. Wuttig Eds., TMS Symp. Proc., Warrendale, PA (1994).
[54] Chou Y. T. and Li J.C.M., *Mathematical Theory of Dislocations*, T. Mura Ed., ASME, New York (1969) 116.
[55] Yoo M. H. and King A. H., *Metall. Trans.* A **21** (1990) 2431.
[56] Chen S. P., Voter A. F. and Srolovitz D. J., *High-Temperature Ordered Intermetallic Alloys II*, I. N. S. Stoloff, C, C, Koch, C. T. Liu and O. Izumi Eds., MRS Symp. Proc. **81**, MRS Pittsburgh, PA (1987) 45.
[57] Foiles S. M., Baskes M. I. and Daw M. S., *Phys. Rev.* B **33** (1986) 7983.
[58] Foiles S. M. and Daw M. S., *J. Mater. Res.* **2** (1987) 5.
[59] Watanabe T., *Intergranular and Interphase Boundaries in Materials*, Ph. Komninou and A. Rocher Eds., *Mater. Sci. Forum* **126-128** (1993) 295..
[60] Hanada S., Ogura T., Watanabe S., Izumi O. and Masumoto T., *Actal Metall.* **34** (1986) 13.
[61] Mathews J. W., *Phil. Mag.* **29** (1974) 797.
[62] Yokoshima S. and Yamaguchi M., *Acta Mater.* **44** (1996) 873.
[63] Heatherly L., George E. P., Liu C. T. and Yamaguchi M., *Intermetallics* (submitted).
[64] Appel F., Chrisroph U. and Wagner R., *Phil. Mag.* A **72** (1995) 341.
[65] Umakoshi Y., Nakano T. and Yamabe Y., *Mater. Sci. Eng.* A**152** (1992) 81.
[66] Hazzledine P. M. and Kad B. K., *Mater. Sci. Eng.* **A192/193** (1995) 340.

[67] Hazzledine P. M. and Rao S. I., *Layered Materials for Structural Applications*, J. J. Lewandowski, C. H. Ward, M. R. Jackson and W. H. Hunt, Jr. Eds., MRS Symp. Proc. **434**, MRS Pittsburgh, PA (1996) 135.
[68] Liu C. T., Schneibel J. H., Maziasz P. J., Wright J. L. and Easton D. S., *Intermetallics* **4** (1996) 429.
[69] Sun Y. Q., *High Temperature Ordered Intermetallic Alloys VII*, C. C. Koch, N. S. Stoloff, C. T. Liu and A. Wanner Eds., MRS Symp. Proc. **460**, MRS Pittsburgh, PA (to be published).
[70] Yoo M. H., *Gamma Titanium Aluminides*, Y.-W. Kim, R. Wagner and M. Yamaguchi Eds., TMS Symp. Proc., Warrendale, PA (1995) 259.

Figure Captions

Fig. 1 Schematic view of self-trapping process of source dislocations bowing out from sub-boundary (from [35]).

Fig. 2 Frank-Read loop formation from (a) a primary source with the anchor points of separation l_0 and (b) the secondary source from a macro-kink with the kink height of h.

Fig. 3 Interaction of dislocations with a grain boundary.

Fig. 4 CSF energies and dissociation of screw $[1\bar{1}0]/2$ dislocations in PST crystals.

Fig. 5 Angular dependence of the stress concentration at an interface of [110] symmetric tilt-boundaries due to $(1\bar{1}1)[10\bar{1}]$ or $(1\bar{1}1)[011]$ dislocation pile-up.

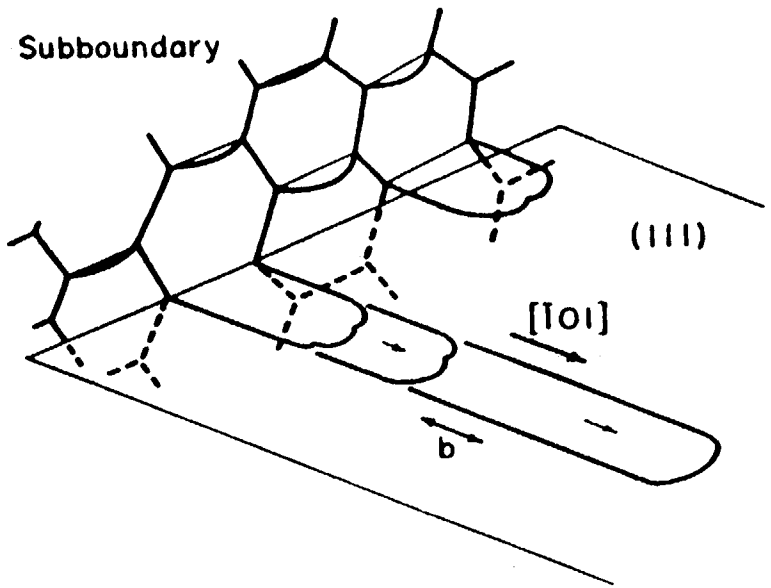

Fig. 1

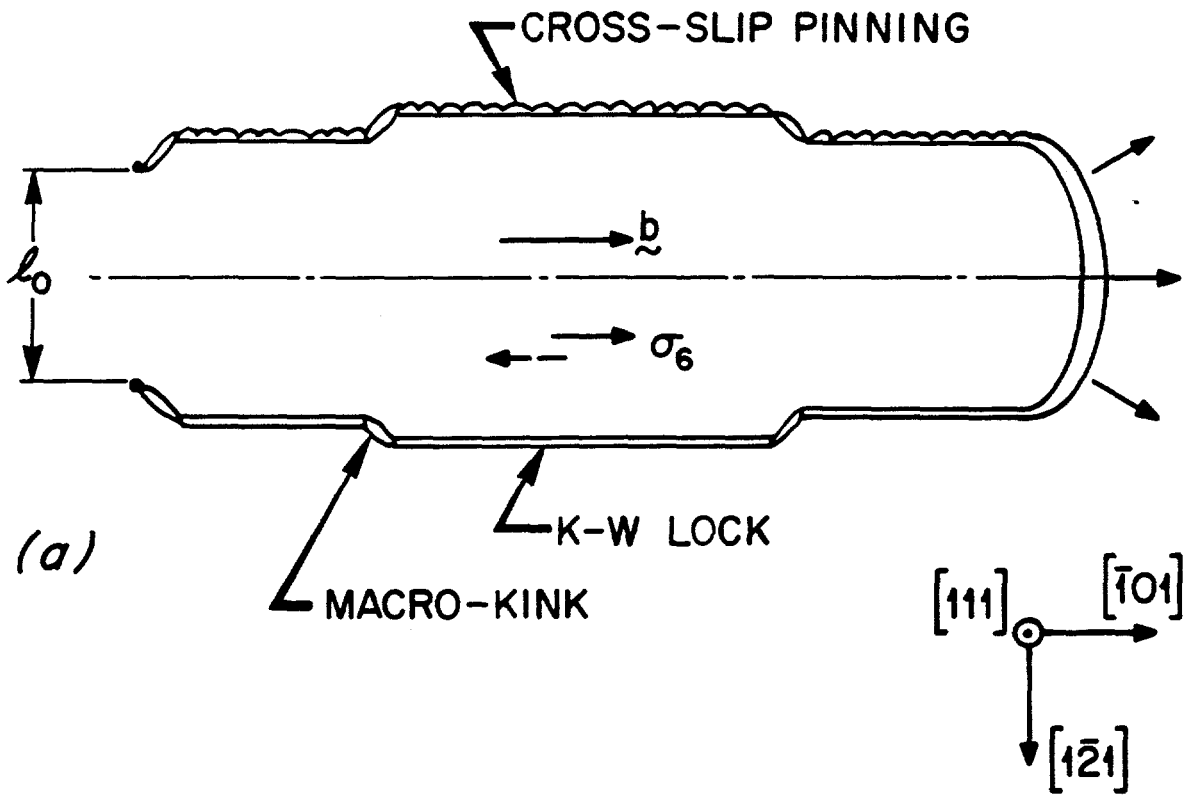
CROSS-SLIP PINNING
ℓ_0
$\underset{\sim}{b}$
σ_6
K-W LOCK
MACRO-KINK
(a)
[111]
[$\bar{1}$01]
[1$\bar{2}$1]

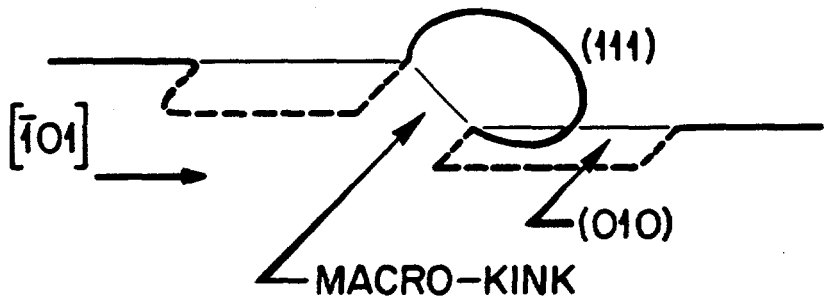
(111)
[$\bar{1}$01]
(010)
MACRO-KINK
(b)

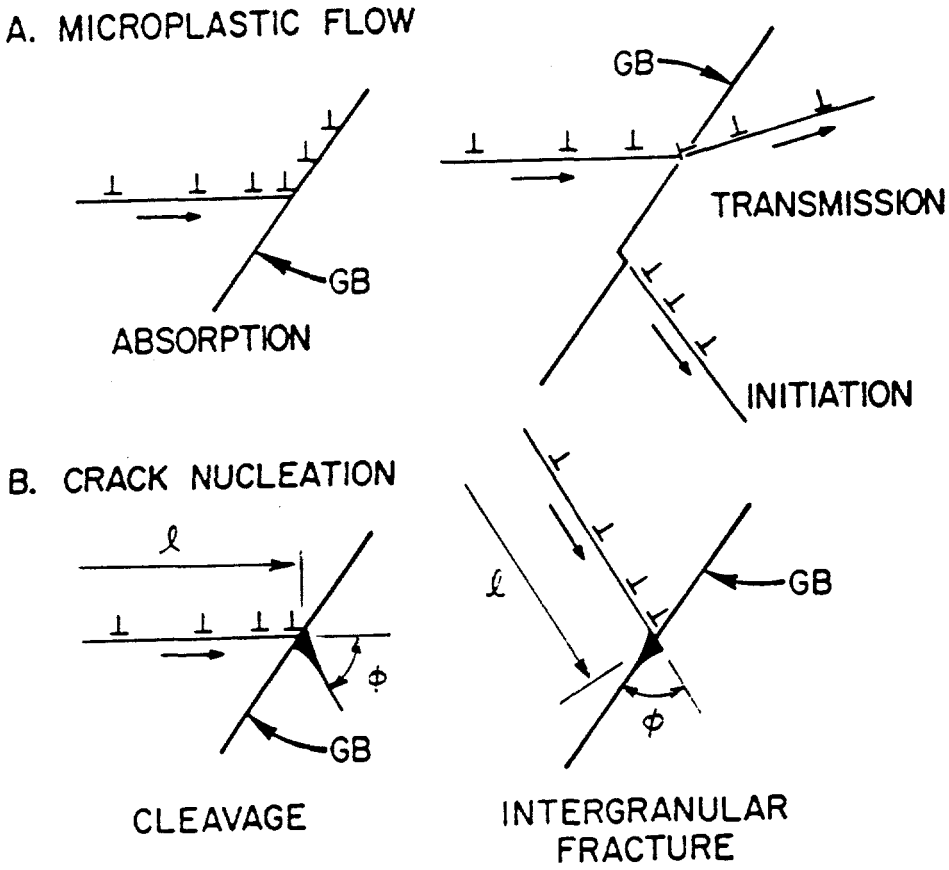
A. MICROPLASTIC FLOW
GB
TRANSMISSION
GB
ABSORPTION
INITIATION
B. CRACK NUCLEATION
ℓ
Φ
GB
ℓ
GB
Φ
CLEAVAGE
INTERGRANULAR
FRACTURE

Fig. 3

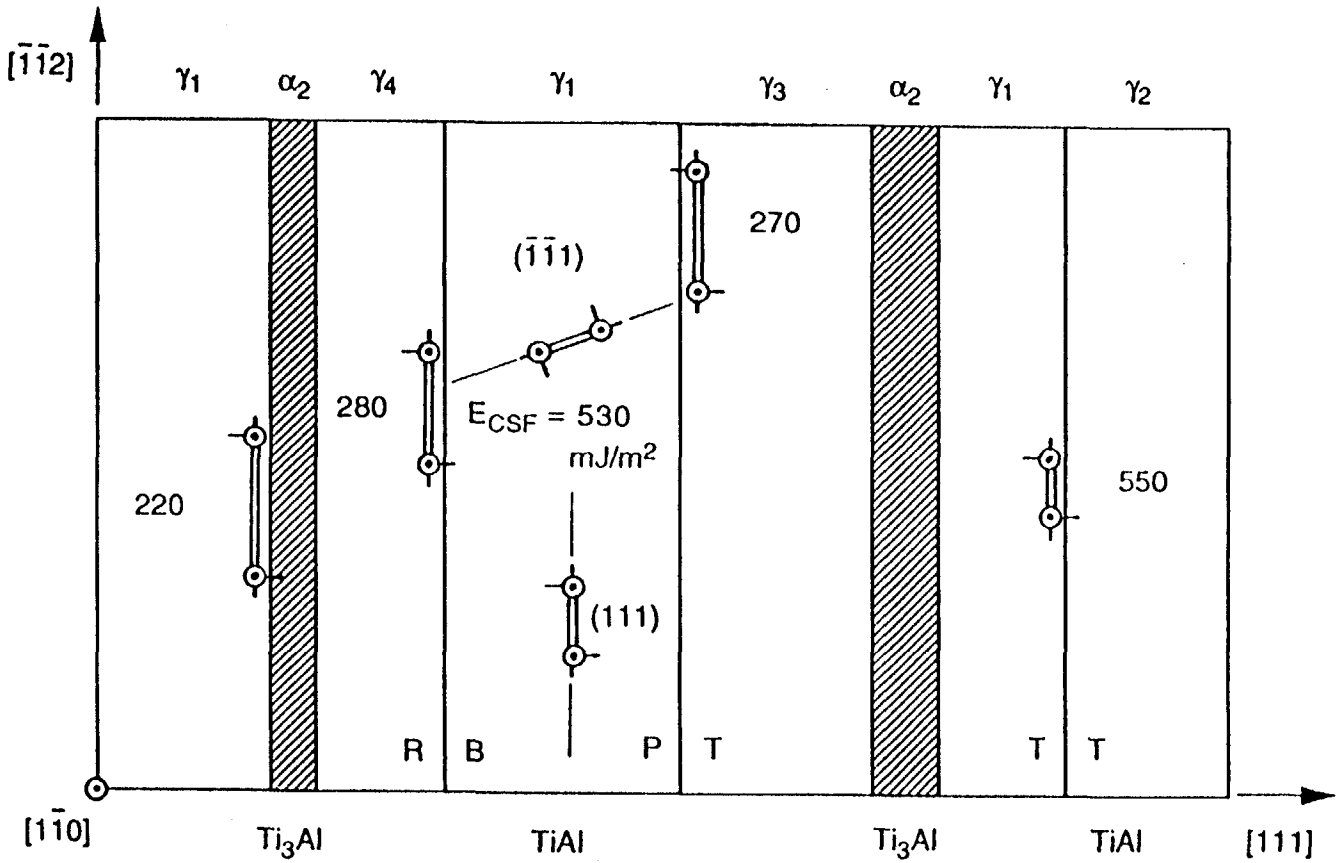
[1̄1̄2]
γ1
α2
γ4
γ1
γ3
α2
γ1
γ2
270
(1̄1̄1)
280
E_CSF = 530
mJ/m²
220
550
(111)
R
B
P
T
T
T
[1̄10]
Ti3Al
TiAl
Ti3Al
TiAl
[111]

Fig. 4

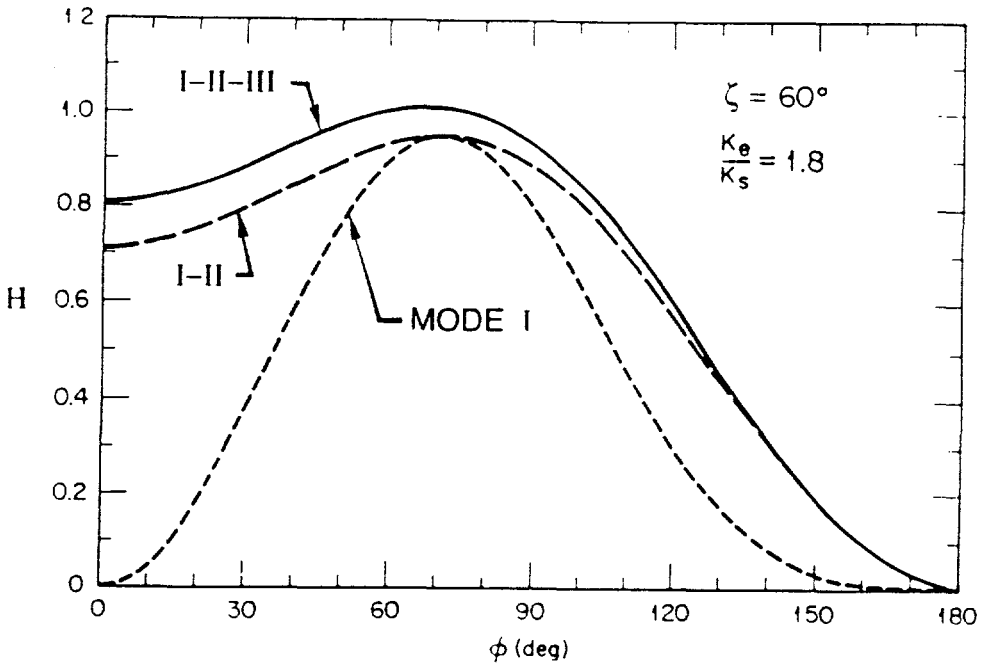
1.2
1.0
0.8
0.6
0.4
0.2
0
H
I–II–III
I–II
MODE I
ζ = 60°
$\frac{K_\theta}{K_s}$ = 1.8
0
30
60
90
120
150
180
φ (deg)

Fig. 5

Table 1. Number of Allowable Reactions at Gbs in the $L1_2$ Structure

	Absorption		Transmission	
	$\Sigma = 3N$	$\Sigma \neq 3N$	$\Sigma = 3N$	$\Sigma \neq 3N$
Disordered	12	6	288	216
Ordered	3	0	72	72
	[Possible 30]		[Possible 1800]	

Table 3. Calculated Shear Fault Energies at the $TiAl/Ti_3Al$ Interface (in Units of mJ/m^2)

Plane	APB	SISF	CSF
(111) TiAl	560	90	530
(0001) Ti_3Al	300		320
$TiAl/Ti_3Al$	280	20	220

Table 2. Interfacial Energies of γ/γ Lamellar Boundaries in TiAl (in Units of mJ/m^2)

Interface type	θ	$\mathbf{f}=0$ Γ_i	$\frac{1}{2}<\bar{1}01]$ APB	$\frac{1}{6}[11\bar{2}]$ SISF	$\frac{1}{6}<\bar{2}11]$ CSF
Bulk	0°	0	560	90	530
Pseudo-twin	60°	270	270	270	270
Rotational	120°	250	250	280	280
True-twin	180°	60	550	60	550

Table 6. Interfacial Fracture Energies in Two-Phase TiAl
(in Units of J/m^2)

Interface	G_c	Γ_i	E_m	G_i
γ/γ				
PT (60°)	4.5	0.27		~4.2
RB (120°)	4.5	0.25	0.03	4.2
TT (180°)	4.5	0.06		~4.4
α_2/γ	4.65	0.10	0.07	4.5

Table 4. Surface Energies and GB Cohesive Energies Calculated Using the EAM (in Units of J/m^2)

	γ_s			G_b
	(111)	(001)	(110)	(HKL)/[001]
Cu	1.17	1.28	1.40	2.0
Al	0.82	0.82	0.96	1.7
Ni	1.45	1.58	1.73	2.9
Ni_3Al	1.65	1.62[a]	1.73[a]	3.0
		1.89[b]	1.92[b]	

*a*Mixed composition planes.
*b*Pure nickel planes.

Table 5. Orientation Factors for Crack Initiation at [110] Symmetric Tilt Boundaries in Ni_3Al (in Units of m^2/J)

Σ	(HKL)	$2H/G_c$			$\frac{2H}{G_b}$
		(111)	(001)	(110)	
3	$(1\bar{1}\bar{1})$	0.56	0.48	0.55	0.49
9	$(2\bar{2}\bar{1})$	0.61	0.48	0.43	0.35
11	$(3\bar{3}\bar{2})$	0.61	0.47	0.50	0.40
17[b]	$(3\bar{3}\bar{4})$	0.52	0.51	0.55	0.55
19[a]	$(3\bar{3}\bar{1})$	0.59	0.50	0.34	0.29
27[a]	$(5\bar{5}\bar{2})$	0.60	0.49	0.38	0.31
33[a]	$(4\bar{4}\bar{1})$	0.56	0.52	0.29	0.26
33[c]	$(5\bar{5}\bar{4})$	0.59	0.47	0.53	0.44
41[c]	$(4\bar{4}\bar{3})$	0.59	0.47	0.52	0.43